Journal of Power Sources 254 (2014) 298–305

Contents lists available at ScienceDirect

Journal of Power Sources

journal homepage: www.elsevier.com/locate/jpowsour

Synthesis of size-selected Pt nanoparticles supported on sulfonated graphene with polyvinyl alcohol for methanol oxidation in alkaline solutions

Jen-Ming Yang [a,*], Sheng-An Wang [a], Chia-Liang Sun [a,b], Ming-Der Ger [c]

[a] Department of Chemical and Materials Engineering, Chang Gung University, Kwei-Shan, Tao-Yuan 333, Taiwan
[b] Biosensor Group, Biomedical Engineering Research Center, Chang Gung University, Kwei-Shan, Tao-Yuan 333, Taiwan
[c] Department of Chemical and Materials Engineering, Chung Cheng Institute of Technology, National Defense University, Dashi, Tao-Yuan 335, Taiwan

HIGHLIGHTS

- Pt nanoparticles are loaded on sulfonated graphene with anionic conductive PVA.
- Methanol oxidation properties of catalysts between PVA and Nafion are compared.
- Pt on sulfonated graphene outperforms those on graphene and XC-72 carbon powders.
- Sulfonate functional groups on graphene can improve the catalytic activities.

ARTICLE INFO

Article history:
Received 18 August 2013
Received in revised form
29 December 2013
Accepted 30 December 2013
Available online 6 January 2014

Keywords:
Graphene
Nanoparticle
Polyvinyl alcohol
Alkaline
Methanol oxidation
Alkaline direct methanol fuel cell

ABSTRACT

In this study, the size-selected platinum (Pt) nanoparticles are loaded on sulfonated graphene with polyvinyl alcohol (PVA) as the conductive polymer for fuel-cell applications. Methanol oxidation reactions and reliability of various catalysts based on carbon black, graphene, and sulfonated graphene catalyst supports are compared under alkaline conditions. When PVA is used as the conductive polymer in place of Nafion, both the electrochemical active surface area (ECSA) and the methanol oxidation property were superior, irrespective of the catalyst and support. On the other hand, the catalyst with Pt on sulfonated graphene (Pt/sG) outperforms those on other supports. For methanol oxidation, the catalyst decay occurs with a decay of only 9.06% for Pt/sG. It is suggested that the sulfonate functional group on graphene not only improves catalytic activity but can also enhance catalyst reliability.

1. Introduction

The prospect of using direct methanol fuel cells (DMFCs) in portable electronic products is favorable due to their high energy density [1,2]. In 1955, during the early developmental stages of DMFCs, Justi and Winsel described a DMFC as being composed of a porous nickel anode and a porous nickel–silver cathode in an alkaline medium. The first DMFC using solid polymer films was designed by Hunger [3]. In addition to high energy density, other advantages to DMFCs include portability, ease of storage, scalability, and low pollutant emissions [4]. Certain limitations hinder the development and application of DMFCs. These limitations include methanol permeability from the anode to the cathode and the low catalytic activity [3]. In alkaline DMFCs, it is essential to both overcome methanol permeability and enhance ionic conductivity. Numerous researchers have utilized different polymers in the synthesis of alkaline ion-exchange membranes, including polyvinylchloride (PVC) [5], polyepichlorohydrin (PECH) [6], polyetherimide (PEI) [7], polybenzimidazole (PBI) [8] and polyvinyl alcohol (PVA) [9–15]. Consequently, the mechanical and electrochemical properties of ion-exchange membranes have been significantly improved. Yang et al. have used polyvinyl alcohol as a substrate [14], which enabled an ionic conductivity as high as 0.11 Scm^{-1} at 25 °C [14]. Various ionic conductivities of polyvinyl alcohol as a substrate are shown in Table S1 with the comparison of Nafion 115. It is worthwhile to mention that the status of proton exchange membrane direct ethanol fuel cells (PEM-DEFCs) and

* Corresponding author. Tel.: +886 3 2118800x5290; fax: +886 3 3274901.
E-mail address: jmyang@mail.cgu.edu.tw (J.-M. Yang).

0378-7753/$ – see front matter © 2014 Elsevier B.V. All rights reserved.
http://dx.doi.org/10.1016/j.jpowsour.2013.12.120

anion exchange membrane direct ethanol fuel cells (AEM-DEFCs) has been reviewed [16].

Because DMFCs exhibit high energy densities and conversion rates, the electrocatalytic oxidation of methanol has been extensively studied [17]. DMFCs with Pt and Pt-based catalysts have demonstrated enhanced efficiency in methanol oxidation and, therefore, have become commonly used in research. The electrocatalytic oxidation of methanol is a complex process because the reaction produces a number of intermediate products and toxic materials. Specifically, the use of Pt and Pt-based catalysts for the electrocatalytic oxidation of methanol under acidic conditions can easily lead to toxic carbon-monoxide-like intermediates [18,19]. The use of alkaline electrolytes in place of acidic electrolytes in fuel cells, however, has been demonstrated to provide significant improvements in performance [19–23]. Nevertheless, the scarce world reserves of Pt and its high price increases the total cost of the system and thus limits the feasibility of fuel cells [24]. In addition, the electrocatalytic activity of methanol oxidation is also influenced by numerous factors, such as the size and dispersion of the catalyst, the characteristics of the catalyst support, and the catalyst preparation method [22,25–28].

The use of a carbon-based material as the catalyst support can improve the reactivity and stability of the catalyst during electrocatalytic oxidation. Carbon-based supports, however, may suffer from catalyst particle sintering and aggregation because of weak interaction between the carbon and the catalyst metals, which reduces the active catalytic area and ultimately results in the loss of performance over a long period of operation [29]. Furthermore, carbon supports are susceptible to corrosion [Eq. (1)], which can facilitate both the loss of the valuable catalyst through detachment and an increase in the aggregation of the catalyst [30]. This process may also result in microstructural damages and changes in the surface reactivity of the catalyst and ultimately lead to a loss of electrochemical surface area (ECSA) [31] and decreased methanol oxidation activity.

$$C + 2H_2O \rightarrow CO_2 + 4H^+ + 4e^- \quad (E^o = 0.207\,V \text{ vs. NHE at } 25\,^\circ C) \tag{1}$$

Because the activity of a catalyst directly corresponds to its accessible surface area, a reduction of the particle size of the catalyst can greatly enhance catalytic activity. Therefore, the particle size effect of the catalyst must be taken into account [32]. The surface and bulk structure of the catalyst support is a crucial factor in the production of high electrocatalytic activity [33–35]. A good support must exhibit good electrical conductivity, a high surface area, high porosity, and excellent corrosion resistance. The previously mentioned properties predominantly alter the dispersibility, stability, and electronic properties of the catalyst. Carbon black was used as a fuel cell catalyst support throughout the 1990s. To increase the electro-catalytic activity and stability of the catalyst, numerous forms of carbon supports were developed in recent years, such as ordered mesoporous carbon (OMC) [36], carbon nanotubes (CNTs) [37–40], carbon gels [41], carbon nanohorns (CNH) [42], carbon nanocoils (CNC) [42], activated carbon fibers (ACFs) [43], carbon nanofibers (CNFs) [44], boron-doped diamonds (BDDs) [45], and graphene [46–59]. Jiang et al. deposited a droplet of polyvinyl alcohol solution directly onto the electrode surface to form a PVA bond [60]. This step was followed by electro-oxidation of ethanol using Pt/C and PtSn/C catalysts in alkaline and acidic solutions. Using the same catalysts, the current generated from the electro-oxidation of ethanol was higher in the alkaline environment than in the acidic environment. Furthermore, the electro-oxidation of ethanol under an open-loop alkaline environment exhibited a lower potential than in the acidic environment. These results indicate that alkaline environments can improve the electro-oxidation efficiency of ethanol [60]. Wang et al. investigated the durability of carbon black and multiwalled CNTs (MWCNTs) as carbon supports under acidic conditions. They found that MWCNTs were more durable and that the platinum surface area and attenuation of the redox activity were diminished [30]. Currently, little is known about the use of PVA as a conductive polymer in an alkaline environment. In this paper, PVA and Nafion were used in an alkaline environment to investigate the reliability of platinum on carbon (Pt–C), platinum on graphene (Pt-G), and platinum on sulfonated graphene (Pt-sG) catalysts using cyclic voltammetry (CV) during the electro-oxidation of methanol.

2. Experimental

2.1. Reagents

The reagents used in this investigation were platinum tetrachloride (99%, Acros Organics), ethylene glycol (99%, J.T. Baker), sulfuric acid (97–99%, Merck G.R.), methanol (99.8%, Fluka), a solution of tetrafluoroethylene-hexafluoropropylene copolymer (5 wt.%, DuPont), polyvinyl alcohol (average molecular weight 70,000–100,000, Sigma–Aldrich), nitrogen (99.99%), carbon dioxide (99.99%), ammonium sulfate (99%, J. T. Baker), and potassium hydroxide (Sigma–Aldrich).

2.2. Synthesis of grapheme oxide and sulfonated graphene

Graphene oxide powders were prepared following Staudenmaier's method and then reduced to graphene powders by annealing at 1050 °C under an argon atmosphere [61,62]. To prepare sulfonated graphene, graphene was added to a solution of aqueous ammonium sulfate (0.001 g in 40 mL of deionized water). The solution was then heated to 235 °C, filtered, and dried [63].

2.3. Preparation of Pt-C, Pt-G and Pt-sG catalysts

A size-selected Pt colloidal solution was synthesized following the procedure as described in previous study [27,64–66]. Carbon black, XC-72R, graphene and sulfonated graphene were separately mixed with the size-selected Pt colloidal solution in a 2 M solution of sulfuric acid and ethylene glycol (1:1 volume ratio) and stirred for 24 h. The mixture was sonicated with an ultrasonic bath (Dleta DC300, 40 kHz and 300 W) for 8 h and filtered and dried for 48 h to yield the Pt/C, Pt/G, and Pt/sG catalysts, respectively. The Pt-C, Pt-G, and Pt-sG catalysts were mixed with deionized water, ethanol, and conductive polymer to generate the catalyst inks, as described previously [64]. The three kinds of catalyst were separately mixed with DI water, ethanol, and Nafion and then ultrasonically treated in order to form Pt/C(Nafion), Pt/G(Nafion), and Pt/sG(Nafion) inks, respectively. When PVA is used instead of Nafion, the three kinds of Pt/C(PVA), Pt/G(PVA), and Pt/sG(PVA) inks were also formed. Approximately 10 μL of the catalyst ink was deposited onto a glassy carbon electrode and allowed to dry at room temperature to modify the electrode. The platinum loading is around 11 μg cm^{-2} in the electrodes.

2.4. Instrumentation and electrochemical measurements

Transmission electron microscopy (TEM, Jeol JEM-1230, 100 kV) was used to characterize the sample morphologies, and an electrochemical analyzer was used to evaluate the electrochemical characteristics. After setting up the three-electrode device (a glassy carbon electrode was used as the working electrode, mercury/mercury oxide was used as the reference electrode, and a platinum

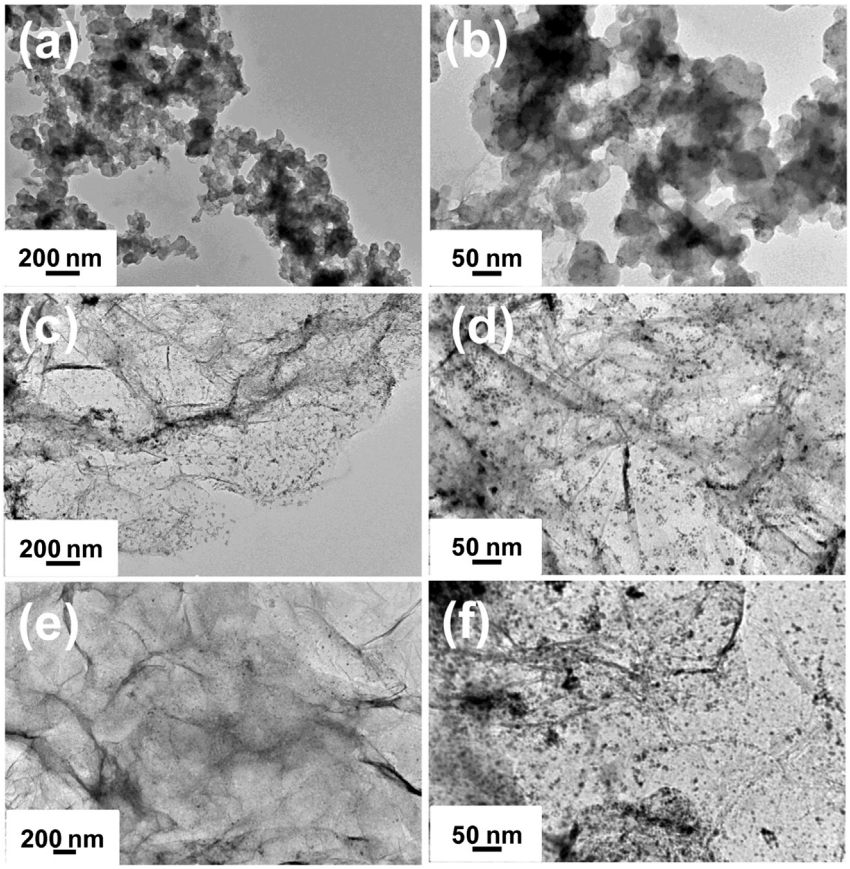

Fig. 1. TEM images of Pt/C(PVA), Pt/G(PVA), and Pt/sG(PVA): (a), (c), and (e) are at 100,000 × magnification; (b), (d), and (f) are at 300,000 × magnification.

coil was used as the auxiliary electrode), a 1 M nitrogen-purged potassium hydroxide solution was passed through the electrode assembly. The measurements were collected with a scan rate of 50 mV s^{-1}, and the potential range was −1.0 to 0.2 V. The above test was repeated for a nitrogen-purged solution of 1 M potassium hydroxide +0.5 M methanol using the same scan rate of 50 mV s^{-1} and the potential range of −1.0 to 0.2 V.

To test the reliability of the fabricated catalysts, each catalyst was subjected to 100 scans at 100 mV s^{-1} under a nitrogen-purged 1 M potassium hydroxide solution. The catalyst was then subjected to a nitrogen-purged 1 M potassium hydroxide +0.5 M methanol electrolyte solution for the electro-oxidation of methanol after the 10th, 25th, 50th, 75th, 100th, 150th, and 200th scans in a standard 1 M potassium hydroxide solution. Finally, the methanol oxidation performance of the catalyst was evaluated by measuring the electrochemical active surface area after each of the previously mentioned scan intervals. The electrochemical active surface area is an important factor in electrochemical measurements; it is often calculated using hydrogen adsorption, desorption isotherms and the following equations:

$$\mathrm{ESA}\left(\mathrm{m^2/g}\right) = \frac{Q_H(\mu\mathrm{C})}{210(\mu\mathrm{Ccm^{-2}}) \times w_{\mathrm{Pt}}(\mathrm{g})} \times \frac{1(\mathrm{m^2})}{10,000(\mathrm{cm^2})} \quad (2)$$

$$\mathrm{ECSA}\left(\mathrm{cm^2}\right) = \frac{Q_H(\mu\mathrm{C})}{210(\mu\mathrm{Ccm^{-2}})} \quad (3)$$

Q_H is the average charge integrated from the hydrogen adsorption/desorption region in a cyclic voltammogram. w_{Pt} is the total weight of Pt used in the catalyst layer.

3. Results and discussion

3.1. Characterization of Pt nanoparticles on various carbon supports

Fig. 1 shows the TEM images of the three catalysts—Pt/C, Pt/G, and Pt/sG—at different magnifications. The distribution of the platinum nanoparticles across the carbon supports can be observed in each image. Most of the platinum nanoparticles are approximately several nanometers in diameter, and as evident in the figure, the density of the attached nanoparticles on the sulfonated graphene is much higher than that on the unsulfonated graphene.

3.2. Effects of various catalyst systems on electrochemical properties

Fig. 2 shows the effects of the addition of PVA and Nafion to each catalyst ink on their cyclic voltammograms. Fig. 2 (a), (b), and (c) show the CV curves for Pt/C, Pt/G, and Pt/sG, respectively, when PVA and Nafion were added as the anionic conductive polymer. Fig. 2 (d) shows the overlay of the CV curves of the three different catalysts. When Nafion was replaced with PVA, which resulted in an increase in ECSA, the value of ECSA for Pt/C(PVA), Pt/G(PVA), and Pt/sG(PVA) are 88.08, 233.62, and 238.37 $m^2 g_{Pt}^{-1}$, respectively. The values of ECSA for the two polymers, Nafion and PVA, systems increase as follow: Pt/C < Pt/G < Pt/sG. Under alkaline conditions, the CV curves can be qualitatively segmented into (1) the underpotential deposited hydrogen zone (H_{und}); (2) the high-potential irreversible oxide formation zone, also known as the irreversible hydrogen adsorption zone ($OH_{ad,\ irrev}$); and (3) the region between the underpotential and the high-potential zones, known as the

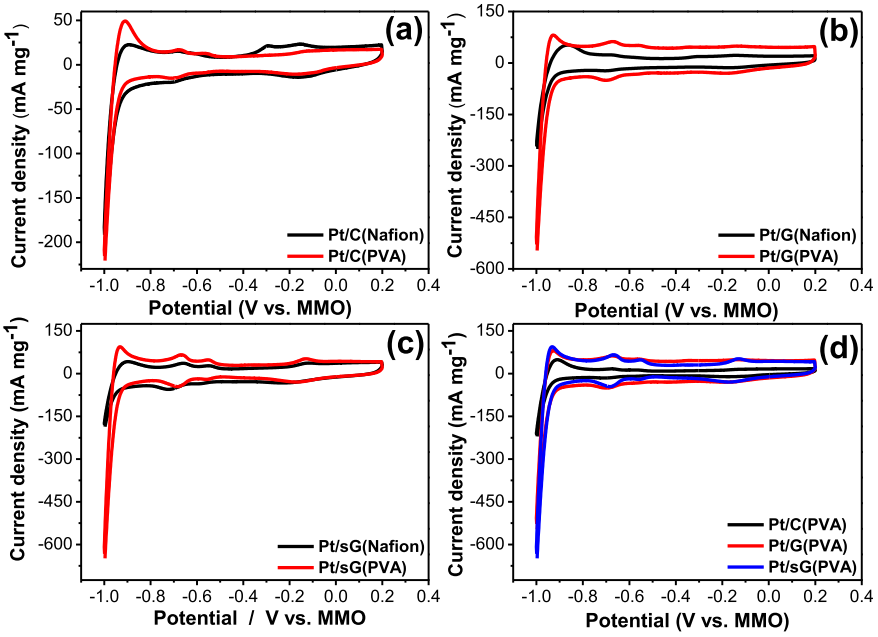

Fig. 2. Effect on the CV curves of the addition of PVA and Nafion to the catalyst inks for (a) Pt/C, (b) Pt/G, and (c) Pt/sG; (d) overlay of all three catalysts (electrolyte: 1 M KOH; scan rate: 50 mV s^{-1}).

reversible hydrogen adsorption zone ($OH_{ad,rev}$) [67]. The overall reaction pathway includes hydrogen desorption, which is immediately followed first by the reversible adsorption of OH and then by irreversible oxide formation [22]. This mechanism was confirmed by titration of the OH_{ad} present at the H_{und} with a CO oxidation reaction [68]. Compared to the structure of Nafion with a sulfonate ionic group, the existence of hydroxyl group in PVA is shown in Scheme 1. It is easy to find that the number of mole percent of hydroxyl group in PVA is higher than that of sulfonate ionic group in Nafion. Due to the higher content of functional group in PVA, the higher values of ECSA were found for the PVA systems than those of Nafion systems.

Fig. 3 shows the effects of the addition of PVA and Nafion to each catalyst ink on the methanol oxidation reaction (MOR). Fig. 3 (a), (b), and (c) show the CV curves for Pt/C, Pt/G, and Pt/sG, respectively, when PVA and Nafion were added as the anionic conductive polymer. The methanol oxidation performance of all three catalysts was measured under alkaline conditions (1 M KOH + 0.5 M MeOH). Based on this figure, the methanol oxidation performance significantly increased when PVA was used in place of Nafion, irrespective of the catalyst used. Fig. 3 (d) shows the overlay of the CV curves for all three catalysts. The driving force for methanol oxidation is dependent on a delicate balance between the rate of dehydrogenation of methanol and the reaction of CO_{ad} [22,69]:

$$CH_3OH_{sol} \rightarrow CH_3OH_{ad} \rightarrow CO_{ad} + 4H^+ + 4e^- \quad (4)$$

The dehydrogenated product CO_{ad} reacts with the electron-donating oxygen species OH_{ad} in an alkaline solution (OH^-):

$$OH^- \rightarrow OH_{ad} + H^+ + e^- \quad (5)$$

and then undergoes a Langmuir–Hinshelwood-type reaction:

$$CO_{ad} + 2OH_{ad} + 3OH^- \rightarrow CO_3^{2-} + 2H_2O + e^- \quad (6)$$

At low potentials, OH_{ad} facilitates catalysis, whereas at high potentials, OH_{ad} suppresses oxide formation. Therefore, an increase in the methanol oxidation performance can be achieved both by an enhancement of the activity of the intermediates and by the removal of the greatest amount of CO_{ad} using the least amount of OH_{ad} [69]. The initiation of catalysis correlates with the adsorption of OH^- ions. From Fig. 3, catalysis was initiated at a lower potential when PVA was used as the anionic conductive polymer in place of Nafion. This result suggests that PVA can more readily conduct OH^- ions, which results in a faster accumulation of OH_{ad} for the removal of CO. From the methanol electrooxidation reaction in alkaline media, it indicates that the initiation of catalysis correlated with the adsorption of OH^- on the catalyst system [69]. By comparing with the structure of Nafion, the interaction between the hydroxyl group of PVA and hydroxide anion by forming the hydrogen bonding [70] will be more significant than that between the sulfonate ionic group in Nafion and hydroxide anion. With both effects of mole percent of functional group of hydroxyl group and hydrogen bonding with hydroxide anion, the values of ECSA and mass activity for PVA systems are higher than those of Nafion system.

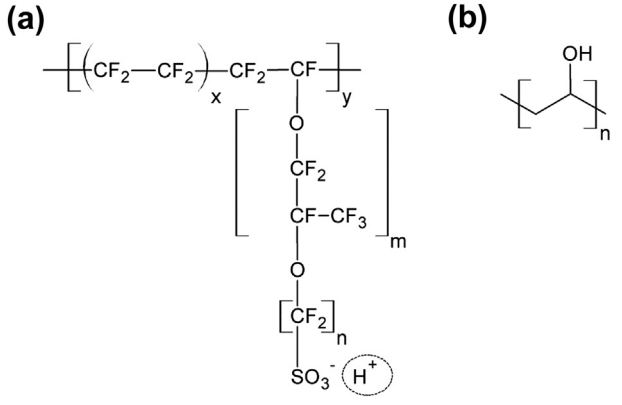

Scheme 1. The structures of (a) Nafion and (b) polyvinyl alcohol (PVA).

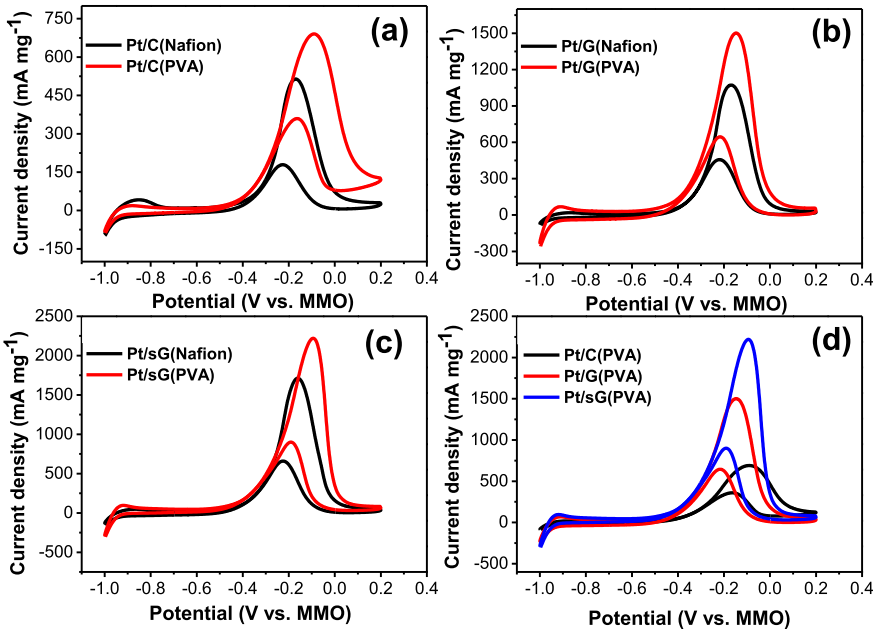

Fig. 3. Effect of the addition of PVA and Nafion to the catalyst ink on the MOR: (a) Pt/C, (b) Pt/G, and (c) Pt/sG; (d) overlay of all three catalysts (electrolyte: 1 M KOH + 0.5 M MeOH; scan rate: 50 mV s^{-1}).

3.3. *Effects of catalyst supports on the reliability*

Fig. 4 shows the CV curves of each catalyst after various numbers of cycles. Fig. 4 (a), (b), and (c) show the CV curves of Pt/C, Pt/G, and Pt/sG, respectively. The influence of the molecular weight of the PVA on each catalyst is noteworthy and the molecular-weight-dependent electrochemical properties were studied and the results showed that the optimal molecular weight of PVA is about 70,000–100,000. The electrochemical active surface areas were calculated from the low-potential hydrogen desorption zone. The hydrogen desorption area decreased with an increase in the number of cycles, and it can be observed from the three figures that the catalyst decay was most severe for Pt/C and least severe for Pt/sG. Fig. 5 shows the MOR curve for each catalyst after various numbers of cycles. This experiment was designed to investigate the reliability of each catalyst when PVA was used as the anionic conductive polymer under alkaline conditions. Fig. 5 (a), (b), and (c) show the MOR curves for Pt/C, Pt/G, and Pt/sG, respectively. Detailed values for each catalyst are summarized in Tables 1–3. As evident in the three panels in Fig. 5, the methanol oxidation performance was greatest at the 50th cycle. This result suggests that the catalyst did not completely activate before the 50th cycle and

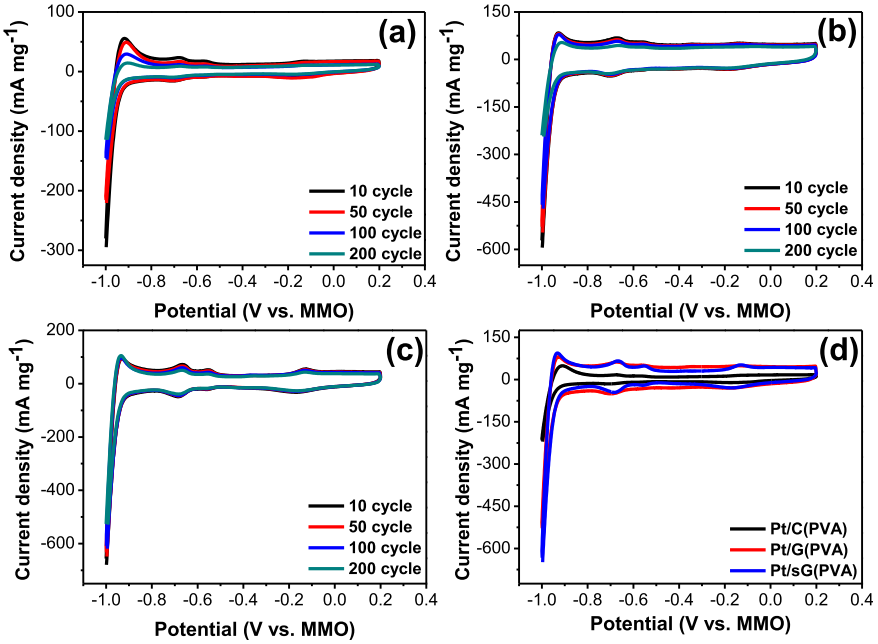

Fig. 4. Effect of the number of cycles on the CV curves for each catalyst: (a) Pt/C(PVA), (b) Pt/G(PVA), and (c) Pt/sG(PVA); (d) overlay of all three catalysts (50th cycle) (electrolyte: 1 M KOH; scan rate: 50 mV s^{-1}).

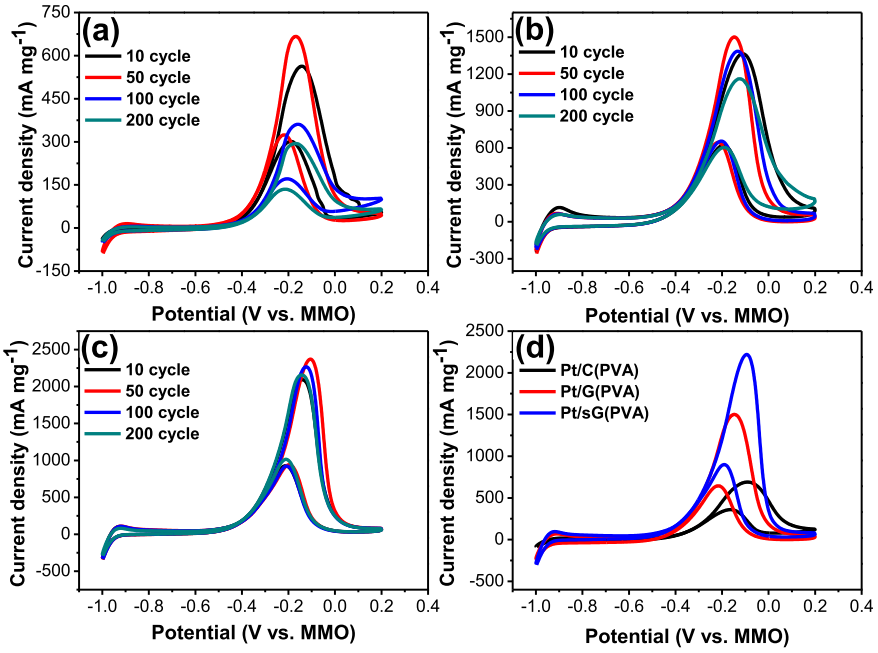

Fig. 5. Effect of the number of cycles on the MOR for each catalyst: (a) Pt/C(PVA), (b) Pt/G(PVA), and (c) Pt/sG(PVA); (d) overlay of all three catalysts (50th cycle) (electrolyte: 1 M KOH + 0.5 M MeOH; scan rate: 50 mV s^{-1}).

that the carbon supports began to corrode after the 50th cycle [28]. Aggregation, sintering, and poisoning of the catalysts caused the decrease in the ECSA, which resulted in decreased methanol oxidation performance [29]. Fig. 6 (a) and (b) show the normalized ECSA and effective surface area (ESA) curves, respectively, from which the hydrogen desorption area of Pt/C was observed to decrease from 112.58 ($m^2g^{-1}_{Pt}$) to 30.03 ($m^2g^{-1}_{Pt}$)—a decay of 73.33%. For Pt/sG, the hydrogen desorption area decreased from 257.58 ($m^2g^{-1}_{Pt}$) to 213.18 ($m^2g^{-1}_{Pt}$)—a decay of only 17.24%. The calculated decay for Pt/G was 30.92%. Based on the ESA decay rate, it can be concluded that graphene provides significantly more resistance against catalyst decay than does carbon black. This result is attributed to the greater surface area of graphene, which enhances the accessibility of Pt. In addition, the sulfonated graphene can further resist catalyst decay, which is attributed to the greater distribution of Pt on this support. Fig. 6 (c) and (d) showed the normalized mass activity and geometric activity of different catalysts after various numbers of cycles, which can be used to elucidate the rate of decay for each catalyst. Not only did Pt/sG exhibit a methanol oxidation performance superior to that of the other two catalysts but its performance only decreased from 2371.31 ($mAmg^{-1}_{Pt}$) to 2156.54 ($mAmg^{-1}_{Pt}$) under repeated cycles—a decay of only 9.06%. The decay for the Pt/C catalyst was as high as 55.89%. These results further confirm that the use of sulfonated graphene as the carbon support not only increases methanol oxidation performance but also significantly enhances

Table 1
Summary of the measured characteristics of the Pt/C(PVA) catalyst support after different numbers of scan cycles.

Cycles	ECSA (cm^2_{Pt})	ESA ($m^2g^{-1}_{Pt}$)	Mass activity ($mAmg^{-1}_{Pt}$)	Geometric activity ($mAcm^{-2}$)	Specific activity ($mAcm^{-2}_{ECSA}$)	If/Ib	MOR onset potential (V)	MOR peak current potential (V)
10	2.67	112.58	563.29	6.80	0.50	1.87	−0.415	−0.143
25	2.63	111.18	609.71	7.36	0.55	2.40	−0.438	−0.151
50	2.08	88.08	666.67	8.05	0.76	2.06	−0.434	−0.169
75	1.91	80.80	470.46	5.68	0.58	2.25	−0.391	−0.137
100	1.42	60.28	361.06	4.36	0.60	2.11	−0.387	−0.160
150	0.97	41.22	334.18	4.04	0.82	2.79	−0.394	−0.177
200	0.71	30.03	294.09	3.55	0.98	2.18	−0.374	−0.171

Table 2
Summary of the measured characteristics of the Pt/G(PVA) catalyst support after different numbers of scan cycles.

Cycles	ECSA (cm^2_{Pt})	ESA ($m^2g^{-1}_{Pt}$)	Mass activity ($mAmg^{-1}_{Pt}$)	Geometric activity ($mAcm^{-2}$)	Specific activity ($mAcm^{-2}_{ECSA}$)	If/Ib	MOR onset potential (V)	MOR peak current potential (V)
10	5.99	253.16	1364.56	16.48	0.54	2.20	−0.467	−0.108
25	5.79	244.54	1454.43	17.56	0.60	2.40	−0.461	−0.119
50	5.53	233.62	1501.69	18.14	0.64	2.33	−0.462	−0.147
75	5.30	223.66	1430.80	17.28	0.64	2.18	−0.453	−0.133
100	5.15	217.67	1385.65	16.73	0.64	2.11	−0.446	−0.134
150	4.51	190.59	1245.15	15.04	0.65	1.97	−0.446	−0.122
200	4.14	174.88	1162.03	14.03	0.67	1.92	−0.445	−0.124

Table 3
Summary of the measured characteristics of the Pt/sG(PVA) catalyst support after different numbers of scan cycles.

Cycles	ECSA (cm^2_{Pt})	ESA ($m^2g^{-1}_{Pt}$)	Mass activity ($mAmg^{-1}_{Pt}$)	Geometric activity ($mAcm^{-2}$)	Specific activity ($mAcm^{-2}_{ECSA}$)	If/Ib	MOR onset potential (V)	MOR peak current potential (V)
10	6.10	257.58	2092.41	25.27	0.81	2.25	−0.485	−0.138
25	5.89	248.82	2275.11	27.48	0.92	2.46	−0.481	−0.124
50	5.64	238.37	2371.31	28.64	1.00	2.52	−0.482	−0.105
75	5.51	232.87	2319.41	28.01	1.00	2.49	−0.481	−0.126
100	5.38	227.15	2267.09	27.38	1.00	2.46	−0.479	−0.124
150	5.10	215.41	2210.13	26.69	1.03	2.43	−0.477	−0.124
200	5.05	213.18	2156.54	26.04	1.01	2.13	−0.484	−0.145

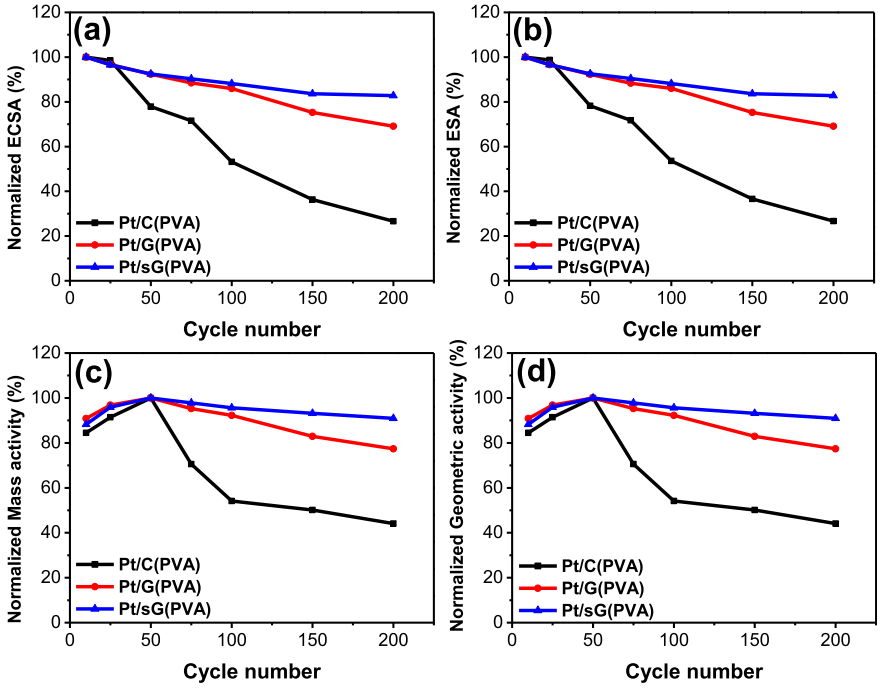

Fig. 6. Comparison of the performance of the catalysts at different cycles: (a) ECSA, (b) ESA, (c) mass activity, and (d) geometric activity.

reliability. This improvement in the methanol oxidation performance is also attributed to the interactive synergy between the metallic catalyst and the sulfonated graphene support [71].

4. Conclusions

In summary, the effects of the use of colloidal Pt nanoparticles, different catalyst supports, and polyvinyl alcohol as the anionic conductive polymer were investigated with respect to methanol oxidation performance. Differences in the methanol oxidation performance were compared for carbon black, graphene, and sulfonated graphene catalyst supports, as well as between polyvinyl alcohol and Nafion as the anionic conductive polymer. Under alkaline conditions, when PVA was used as the anionic conductive polymer in place of Nafion, both the ECSA and the methanol oxidation performance were superior, irrespective of the catalyst and support. In reliability tests, not only did Pt/sG out-perform Pt/C and Pt/G in ESA, the catalyst decay also dropped from 73.33% to 17.24% when Pt/sG was used in place of carbon black. These results suggest that sulfonated graphene can increase the dispersibility of the Pt catalyst and increase its accessibility. For methanol oxidation, the maximum performance was attained after the 50th cycle, which suggests that all catalysts had been fully activated at that time. Catalyst decay was observed to occur after the 50th cycle, with a decay of 55.89% for Pt/C; this value was reduced to 9.06% when Pt/sG was used. This result also confirms that sulfonated graphene not only increases catalytic activity but can also enhance catalyst reliability.

Acknowledgements

We thank the National Science Council, Chang Gung University, and Chang Gung Memorial Hospital for financially supporting this research.

Appendix A. Supplementary data

Supplementary data related to this article can be found at http://dx.doi.org/10.1016/j.jpowsour.2013.12.120.

References

[1] R. Dillon, S. Srinivasan, A.S. Aricò, V. Antonucci, J. Power Sources 127 (2004) 112–126.
[2] A.S. Aricò, V. Baglio, E. Modica, A. Di Blasi, V. Antonucci, Electrochem. Commun. 6 (2004) 164–169.
[3] H. Liu, J. Zhang, Electrocatalysis of Direct Methanol Fuel Cells, Wiley-VCH, Weinheim, 2009.
[4] J. Zhang, G.-P. Yin, Z.-B. Wang, Q.-Z. Lai, K.-D. Cai, J. Power Sources 165 (2007) 73–81.
[5] J. Hu, C. Zhang, J. Cong, H. Toyoda, M. Nagatsu, Y. Meng, J. Power Sources 196 (2011) 4483–4490.

[6] T.Y. Guo, Q.H. Zeng, C.H. Zhao, Q.L. Liu, A.M. Zhu, I. Broadwell, J. Memb. Sci. 371 (2011) 268–275.
[7] G. Wang, Y. Weng, D. Chu, D. Xie, R. Chen, J. Memb. Sci. 326 (2009) 4–8.
[8] H. Hou, G. Sun, R. He, B. Sun, W. Jin, H. Liu, Q. Xin, Int. J. Hydrogen Energy 33 (2008) 7172–7176.
[9] C.C. Yang, J. Power Sources 109 (2002) 22–31.
[10] C.C. Yang, S.J. Lin, S.T. Hsu, J. Power Sources 122 (2003) 210–218.
[11] J.M. Yang, H.Z. Wang, C.C. Yang, J. Memb. Sci. 322 (2008) 74–80.
[12] C.C. Yang, Y.J. Lee, J.M. Yang, J. Power Sources 188 (2009) 30–37.
[13] C.C. Yang, J.M. Yang, C.Y. Wu, J. Power Sources 191 (2009) 669–677.
[14] J.M. Yang, C.Y. Chiang, H.Z. Wang, C.C. Yang, J. Memb. Sci. 341 (2009) 186–194.
[15] J.M. Yang, H.C. Chiu, J. Memb. Sci. 419–420 (2012) 65–71.
[16] A. Brouzgou, A. Podias, P. Tsiakaras, J. Appl. Electrochem. 43 (2013) 119–136.
[17] X.-Z. Fu, Y. Liang, S.-P. Chen, J.-D. Lin, D.-W. Liao, Catal. Commun. 10 (2009) 1893–1897.
[18] Z. Liu, X. Zhang, L. Hong, Electrochem. Commun. 11 (2009) 925–928.
[19] R. Parsons, T. VanderNoot, J. Electroanal. Chem. 257 (1988) 9–45.
[20] C. Susut, T.D. Nguyen, G.B. Chapman, Y. Tong, Electrochim. Acta 53 (2008) 6135–6142.
[21] Y.-W. Lee, S.-B. Han, K.-W. Park, Electrochem. Commun. 11 (2009) 1968–1971.
[22] A.V. Tripkovi, K.D. Popovi, B.N. Grgur, B. Blizanac, P.N. Ross, N.M. Markovi, Electrochim. Acta 47 (2002) 3707–3714.
[23] E. Antolini, E.R. Gonzalez, J. Power Sources 195 (2010) 3431–3450.
[24] A. Brouzgou, S.Q. Song, P. Tsiakaras, Appl. Catal. B Environ. 127 (2012) 371–388.
[25] A. Gamez, D. Richard, P. Gallezot, F. Gloaguen, R. Faure, R. Durand, Electrochim. Acta 41 (1996) 307–314.
[26] M.-W. Xu, G.-Y. Gao, W.-J. Zhou, K.-F. Zhang, H.-L. Li, J. Power Sources 175 (2008) 217–220.
[27] C. Bock, C. Paquet, M. Couillard, G.A. Botton, B.R. MacDougall, J. Am. Chem. Soc. 126 (2004) 8028–8037.
[28] H.A. Gasteiger, N. Markovic, P.N. Ross Jr., E.J. Cairns, J. Electrochem. Soc. 141 (1994) 1795–1803.
[29] R. Kou, Y. Shao, D. Mei, Z. Nie, D. Wang, C. Wang, V.V. Viswanathan, S. Park, I.A. Aksay, Y. Lin, Y. Wang, J. Liu, J. Am. Chem. Soc. 133 (2011) 2541–2547.
[30] X. Wang, W. Li, Z. Chen, M. Waje, Y. Yan, J. Power Sources 158 (2006) 154–159.
[31] S.-Y. Huang, P. Ganesan, B.N. Popov, Appl. Catal. B Environ. 102 (2011) 71–77.
[32] A. Kabbabi, F. Gloaguen, F. Andolfatto, R. Durand, J. Electroanal. Chem. 373 (1994) 251–254.
[33] D.-J. Guo, H.-L. Li, J. Electroanal. Chem. 573 (2004) 197–202.
[34] K.M. Kost, D.E. Bartak, B. Kazee, T. Kuwana, Anal. Chem. 62 (1990) 151–157.
[35] K. Kinoshita, J. Electrochem. Soc. 137 (1990) 845–848.
[36] L. Calvillo, M.J. Lázaro, E. García-Bordejé, R. Moliner, P.L. Cabot, I. Esparbé, E. Pastor, J.J. Quintana, J. Power Sources 169 (2007) 59–64.
[37] T. Maiyalagan, B. Viswanathan, U.V. Varadaraju, Electrochem. Commun. 7 (2005) 905–912.
[38] C.-L. Sun, L.-C. Chen, M.-C. Su, L.-S. Hong, O. Chyan, C.-Y. Hsu, K.-H. Chen, T.-F. Chang, L. Chang, Chem. Mater. 17 (2005) 3749–3753.
[39] C.-L. Sun, Y.-K. Hsu, Y.-G. Lin, K.-H. Chen, C. Bock, B. MacDougall, X. Wu, L.-C. Chen, J. Electrochem. Soc. 156 (2009) B1249–B1252.
[40] C.L. Sun, C.W. Pao, H.M. Tsai, J.W. Chiou, S.C. Ray, H.W. Wang, M. Hayashi, L.C. Chen, H.J. Lin, J.F. Lee, L. Chang, M.H. Tsai, K.H. Chen, W.F. Pong, Nanoscale 5 (2013) 6812–6818.
[41] C. Moreno-Castilla, F.J. Maldonado-Hódar, Carbon 43 (2005) 455–465.
[42] N. Sano, S.-I. Ukita, Mater. Chem. Phys. 99 (2006) 447–450.
[43] E. Yoo, T. Okada, T. Kizuka, J. Nakamura, J. Power Sources 180 (2008) 221–226.
[44] C.A. Bessel, K. Laubernds, N.M. Rodriguez, R.T.K. Baker, J. Phys. Chem. B 105 (2001) 1115–1118.
[45] A.E. Fischer, G.M. Swain, J. Electrochem. Soc. 152 (2005) B369–B375.
[46] Y. Li, L. Tang, J. Li, Electrochem. Commun. 11 (2009) 846–849.
[47] E. Yoo, T. Okata, T. Akita, M. Kohyama, J. Nakamura, I. Honma, Nano Lett. 9 (2009) 2255–2259.
[48] S. Guo, S. Dong, E. Wang, ACS Nano 4 (2010) 547–555.
[49] Y. Li, W. Gao, L. Ci, C. Wang, P.M. Ajayan, Carbon 48 (2010) 1124–1130.
[50] L. Dong, R.R.S. Gari, Z. Li, M.M. Craig, S. Hou, Carbon 48 (2010) 781–787.
[51] E.G. Castro, R.V. Salvatierra, W.H. Schreiner, M.M. Oliveira, A.J.G. Zarbin, Chem. Mater. 22 (2010) 360–370.
[52] S. Bong, Y.R. Kim, I. Kim, S. Woo, S. Uhm, J. Lee, H. Kim, Electrochem. Commun. 12 (2010) 129–131.
[53] L. Wang, C. Tian, H. Wang, Y. Ma, B. Wang, H. Fu, J. Phys. Chem. C. 114 (2010) 8727–8733.
[54] C.V. Rao, A.L.M. Reddy, Y. Ishikawa, P.M. Ajayan, Carbon 49 (2011) 931–936.
[55] Y. Zhao, L. Zhan, J. Tian, S. Nie, Z. Ning, Electrochim. Acta 56 (2011) 1967–1972.
[56] Y.W. Hsu, T.K. Hsu, C.L. Sun, Y.T. Nien, N.W. Pu, M.D. Ger, Electrochim. Acta 82 (2012) 152–157.
[57] R. Yue, Q. Zhang, C. Wang, Y. Du, P. Yang, J. Xu, Electrochim. Acta 107 (2013) 292–300.
[58] C.L. Sun, W.C. Cheng, T.K. Hsu, C.W. Chang, J.L. Chang, J.M. Zen, Electrochem. Commun. 30 (2013) 91–94.
[59] C.L. Sun, J.S. Su, J.H. Tang, M.C. Lin, J.J. Wu, N.W. Pu, G.N. Shi, M.D. Ger, J. Taiwan Inst. Chem. Eng. (2013), http://dx.doi.org/10.1016/j.jtice.2013.08.011.
[60] L. Jiang, A. Hsu, D. Chu, R. Chen, Int. J. Hydrogen Energy 35 (2010) 365–372.
[61] C.L. Sun, C.T. Chang, H.H. Lee, J. Zhou, J. Wang, T.K. Sham, W.F. Pong, ACS Nano 5 (2011) 7788–7795.
[62] L. Staudenmaier, Ber. Dtsch. Chem. Ges. 31 (1898) 1481–1487.
[63] H.-H. Lee, J.-S. Su, M.-C. Lin, C.-L. Sun, H.-W. Wang, M.-D. Ger, K. Dudeck, G. Botton, (unpublished results).
[64] C.-L. Sun, H.-H. Lee, J.-M. Yang, C.-C. Wu, Biosens. Bioelectron. 26 (2011) 3450–3455.
[65] F. Taufany, C.-J. Pan, H.-L. Chou, J. Rick, Y.-S. Chen, D.-G. Liu, J.-F. Lee, M.-T. Tang, B.-J. Hwang, Chem. Eur. J. 17 (2011) 10724–10735.
[66] Y. Chen, J. Wang, H. Liu, M.N. Banis, R. Li, X. Sun, T.-K. Sham, S. Ye, S. Knights, J. Phys. Chem. C. 115 (2011) 3769–3776.
[67] T.J. Schmidt, P.N. Ross Jr., N.M. Markovic, J. Electroanal. Chem. 524–525 (2002) 252–260.
[68] T.J. Schmidt, P.N. Ross, N.M. Markovic, J. Phys. Chem. B 105 (2001) 12082–12086.
[69] A.V. Tripković, S. Štrbac, K.D. Popovi&cacute, Electrochem. Commun. 5 (2003) 484–490.
[70] D. Marx, A. Chandra, M.E. Tuckerman, Chem. Rev. 110 (2010) 2174–2216.
[71] X. Wang, C. Hu, Y. Xiong, H. Liu, G. Du, X. He, J. Power Sources 196 (2011) 1904–1908.